Published in final edited form as:

ACS Appl Mater Interfaces. 2017 April 26; 9(16): 14478–14489. doi:10.1021/acsami.6b15006.

Reverse Microemulsion-Based Synthesis of (Bis)phosphonate-Metal Materials with Controllable Physical Properties: An Example Using Zoledronic Acid-Calcium Complexes

Xu Li, **Youssef W. Naguib**, **Solange Valdes**, **Stephanie Hufnagel**, and **Zhengrong Cui***

The University of Texas at Austin, College of Pharmacy, Division of Pharmaceutics, Austin, Texas, 78712

Abstract

The development of phosphonate-metal materials is tightly related to the advancement in their synthesis methods. Herein, using zoledronic acid (Zol), a bisphosphonate (bioacitve phosphonate with a 'P-C-P' structure), and calcium as model molecules, we applied the reverse microemulsion (RM) method to synthesize a series of Zol-Ca complexes. We comprehensively i) studied the relationship between RM conditions, including the component ratio of RM, co-surfactants, reaction time, reactant concentrations, reaction temperature, and the presence of a phospholipid, 1, 2-dioleoyl-sn-glycero-3-phosphate acid (DOPA), and the physical properties of the complexes synthesized (i.e. shape, size, uniformity, monodispersity and hydrophilicity/hydrophobicity), and ii) explored the underlying mechanism(s). To evaluate the biomedical application potential of the Zol-Ca complexes synthesized, one type of hydrophobic, DOPA-coated spherical Zol-Ca complexes (denoted as Zol-Ca@DOPA) was formulated into a PEGylated lipid-based nanoparticle formulation (i.e. Zol-Ca@bi-lipid NPs, ~24 nm in diameter). In a mouse model with orthotopic mammary tumors, the Zol-Ca@bi-lipid NPs significantly enhanced the distribution of Zol in tumors, as compared to free Zol. It is expected that the RM-based systhesis of (bis)phosphonate-metal materials with controllable physical properties will help expand their applications.

Graphical abstract

*Author of correspondence: Tel: (512) 495-4758, Zhengrong.cui@austin.utexas.edu.

Authors' Contributions:

X. L.: Experimental design, Figures 1–8, Figure S1–S6, Table S1, and writing the paper; Y.N.: Figure 8C, Figure S5; S.V.: Figure 8D; S.H.: Table S1; Z.C.: Experimental design, writing and editing the paper.

Supporting Information

TEM images of Zol-Ca complexes formed in reverse microemulsion with single co-surfactant or different reaction time; proposed structure of Zol-Ca@bi-lipid NPs and their representative TEM images; in vivo release profile of Zol from Zol-Ca@bi-lipid NPs; fluorescent images showing the uptake of Zol in orthotopic M-Wnt mammary tumors; TEM images of other DOPA-coated bisphosphonate-metal complexes, including DOPA-coated alendronic acid-calcium (Ale-Ca@DOPA), clodronic acid-calcium (Clo-Ca@DOPA) and zoledronic acid-zinc (Zol-Zn@DOPA); and the chemical composition (i.e. Ca/Zol ratio) of three selected Zol-Ca complexes.

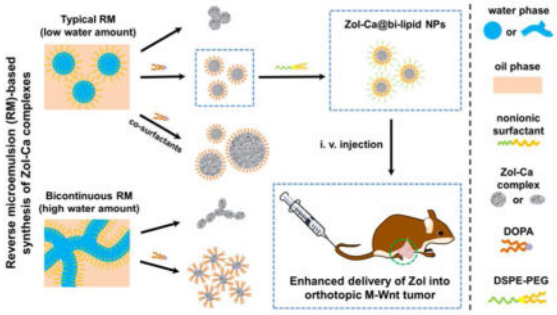

Keywords

Microemulsion compositions; Reaction conditions; Formation mechanism; Nanoparticles; Distribtuion in tumor

Introduction

Phosphonates, including bisphosphonates, are derivatives of organophosphorus acids that contain unique 'P-C' bond(s).[1] In the late 1970s, it was demonstrated that phosphonates are able to coordinate a variety of metal cations to form covalent 'P-O-metal' bonds.[2] Subsequently, the chemistry of phosphonate-metal materials underwent an impressive development, resulting in the generation of numerous functional materials with a broad range of industrial and biomedical applications.[3–7]

Phosphonate-metal materials are generally synthesized by the co-precipitation method (i.e. mixing reactants directly into a mixture of water/polar organic solvent).[8] Modification of reaction conditions, such as temperature, pH value, solvent type and ratio, can influence the coordination manner between phosphonates and metal cations, thereby inducing the generation of numerous crystal structures.[9–10] In recent years, classic sol-gel method has also been used to synthesize porous phosphonate-metal complexes,[11–12] and the 'template-free' and 'surfactant-assisted' strategies have been applied to adjust the porous characteristics (e.g. porosity, pore size) of the resultant phosphonate-metal materials. [13–15] The phosphonate-metal materials synthesized by those methods often have unique crystal structures and desired porous characteristics, but are usually bulk complexes with irregular shapes and poor uniformity and dispersity.[1, 12] A method of synthesizing phosphonate-metal materials with controllable physical properties (e.g. shape, size, uniformity, dispersity) may help expand the potential applications of such materials.

Reverse microemulsion (RM) technology has been utilized to synthesize a wide variety of nanomaterials (e.g. metallic nanoparticles, semiconductor quantum dots, polymeric nanoparticles), and the physical properties of the resultant nanomaterials can be readily controlled by adjusting the parameters of the RM systems.[16–18] There are, indeed, a few reports of synthesizing phosphonate-metal materials by reacting compounds containing phosphonate moiety, e.g. phosphonate-modified cisplatin prodrugs or bisphosphonates, with metal cations in RM systems.[19–21] However, comprehensive studies are needed to correlate

the parameters of the RM systems with the physical properties of phosphonate-metal materials synthesized and to clarify the underlying mechanisms.

The primary aim of the present study was to comprehensively investigate the controlled synthesis of phosphonate-metal materials by RM technology, using zoledronic acid (Zol), a bisphosphonate, and calcium as model molecules. The effects of the component ratios in the RM system (i.e. water/nonionic surfactant/oil), co-surfactant(s), reaction time, reaction temperature, reactant concentration and the inclusion of an anionic phospholipid, 1, 2-dioleoyl-sn-glycero-3-phosphate acid (DOPA) on the shape, size, uniformity and monodispersity of the Zol-Ca complexes synthesized were evaluated. Importantly, the mechanisms underlying the formation of Zol-Ca complexes with various physical properties were discussed. In addition, since there is great interest in applying bisphosphonates such as Zol for tumor therapy,[21–27] we preliminarily evaluated the potential of using the Zol-Ca complexes synthesized to enhance the delivery of Zol into tumors in a mouse model.

Materials and methods

Reagents

Zoledronic acid (zoledronate or Zol) monohydrate, alendronic acid (alendronate or Ale) and disodium clodronic acid (clodronate or Clo) tetrahydrate were from TCI America (Portland, OR). Alexa Fluor 647 (AF647)-labeled Zol was from BioVinc LLC (Los Angeles, CA). Sodium hydrate, calcium chloride, zinc chloride, sodium dihydrogen phosphate, sodium hydrogen phosphate, uranyl acetate (UA) dihydrate, formic acid, formalin, collagenase IV, paraformaldehyde, polyoxymethylene, 3-(4,5-dimethylthiazol-2-yl)-2,5-diphenyltetrazolium bromide (MTT), polyoxyethylene (5) nonylphenylether (NP-5) and polyoxyethylene (10) octylphenyl ether (OEP-10) were from Sigma-Aldrich (St. Louis, MO). DOPA monosodium salt and 1, 2-distearoyl-*sn*-glycero-3-phosphoethanolamine-N-[methoxy (polyethylene glycol)-2000] (DSPE-PEG_{2K}) were from Avanti Polar Lipid, Inc. (Alabaster, AL). Cyclohexane, dimethyl sulfoxide, hexanol, chloroform and ethanol were from Thermo Fisher Scientific Co. (Pittsburgh, PA). APC-labeled anti-mouse CD206 (MMR) antibody was from BioLegend Co. (San Diego, CA). All reagents were used without further purification.

Cells and Animals

J774A.1 murine macrophages were from the American Type Culture Collection (Manassas, VA) and cultured in Dulbecco's Modified Eagle Medium (DMEM) supplemented with 10% fetal bovine serum (FBS), 100 U/mL of penicillin plus 100 μg/mL of streptomycin (1% P/S) at 37 °C and 5% CO_2. MMTV-M-Wnt-1 (M-Wnt) mammary tumor cells (basal-like, triple-negative, claudin-low) were isolated from the spontaneous mammary tumors in MMTV-Wnt-1 transgenic mice with a congenic C57BL/6 background. Such tumor contains a high population of tumor-associated macrophages (TAMs).[28] M-Wnt cells were cultured in RPMI 1640 containing 10% FBS and 1% P/S. All cell culture media and reagents were from Invitrogen (Carlsbad, CA).

Female C57BL/6 mice (6–8 weeks) were from Charles River Laboratories (Wilmington, MA). Animal studies were performed in accordance with the National Research Council Guide for the Care and Use of Laboratory Animals. Animal protocol was approved by the Institutional Animal Care and Use Committee at The University of Texas at Austin. M-Wnt tumor model was established by injecting M-Wnt tumor cells (1×10^6 cells per mouse) into the fourth mammary fat pad of C57BL/6 mice.

Synthesis of Zol-Ca complexes using the RM method

For a typical synthesis of Zol-Ca complexes, surfactant NP-5 was first dissolved in cyclohexane to obtain a homogeneous mixture. Thereafter, an aqueous solution of $CaCl_2$ (0.15 M, pH ~7) or Zol (0.02 M, pH ~9) was added dropwise into such mixture with magnetic stirring, followed by sonication in water bath until the system became transparent. Afterwards, such two types of RM, one containing $CaCl_2$ and the other containing Zol, were mixed with each other to initiate the reaction between $CaCl_2$ and Zol. After a pre-designed time period (i.e. 0.5, 4, 16 or 44 h) at room temperature (~22 °C), the mixed RM was transferred into abundant ethanol, and the resultant mixture was centrifuged at 12 000 × g for 30 min. The precipitate was washed using ethanol twice and re-suspended in ethanol. To comprehensively study the synthesis of Zol-Ca complexes by the RM method, the effects of several reaction parameters on the physical properties of the complexes were evaluated, including the volume ratio of H_2O/surfactant/cyclohexane, co-surfactants (OEP-10 and hexanol), reactant (i.e. $CaCl_2$ or Zol) concentrations in the RM, and reaction temperature.

The morphology of all Zol-Ca complexes synthesized was characterized using an FEI Tecnai Transmission Electron Microscope (TEM) available in the Institute for Cellular and Molecular Biology Microscopy and Imaging Facility at The University of Texas at Austin and operated with high tension of 80 kV. The samples of Zol-Ca complexes were suspended in ethanol, and 6 μL of the suspension was placed onto a carbon film-coated copper grid, followed by observation after dryness.

Determination of the chemical composition of Zol-Ca complexes

To determine the Zol/Ca ratios in the resultant Zol-Ca complexes, such complexes were dissolved in a formic acid/water mixture (0.2%, v/v). The concentration of Zol in the solution was determined directly by ion-exchange high performance liquid chromatography (IE-HPLC, 1260 Infinity II LC System from Agilent Technologies, Santa Clara, CA) with an IC-Pak Anion HC Column (4.6 × 150 mm and 10 μm, Waters Corp., Milford, MA). The mobile phase of IE-HPLC was 0.2% formic acid solution (pH ~3), and the absorption wavelength and the flow rate were 210 nm and 1.8 mL/min, respectively.[29] The calcium concentration in the same solution was determined by inductively coupled plasma mass spectrometry (ICP-MS, Agilent 7500ce), after appropriate dilution using 2% nitric acid.

Preparation and characterization of DOPA-coated Zol-Ca complexes composites

For the preparation of DOPA-coated Zol-Ca composites, the component ratio of $V_{NP\text{-}5}$/$V_{cyclohexane}$ in RM was fixed at 30/70 and the $V_{H_2O}/V_{NP\text{-}5}$ ratio was changed from 1/13.3 to 1/1.5. To prepare the RM, an aqueous solution of reactant ($CaCl_2$ or Zol) was added into 8 mL mixture of NP-5 and cyclohexane. The concentrations of $CaCl_2$ or Zol in the aqueous

solution were 0.15 M and 0.02 M, respectively. DOPA was dissolved in $CHCl_3$ to a concentration of 50 mM. When DOPA was added before the initiation of reaction, 0.12 mL DOPA solution was added dropwise into the Zol-containing RM to reach a final concentration of 0.9 mM. After sonication for several minutes and stirring for 10 min, this RM was mixed together with $CaCl_2$-containing RM. When DOPA was added after the initiation of reaction, 0.12 mL DOPA was directly added into the reaction mixture 4 h after the reaction was started to reach a final concentration of 0.45 mM. After ~16 h of reaction, abundant ethanol was applied to break the RM. The white precipitate was collected, washed with ethanol twice, and then dried. Thereafter, $CHCl_3$ was added to re-suspend the dried precipitates for further TEM characterization.

To purify spherical DOPA-coated Zol-Ca complexes for further studies, the suspension was passed through a 0.22 μm filter and dialyzed against $CHCl_3$ for 48 h in a benzoylated dialysis tube (2 KDa MWCO, Sigma-Aldrich) and then stored at −20 °C.

The concentration of Zol in the Zol-Ca@DOPA storage suspension was determined by IE-HPLC. Due to the high hydrophobicity of Zol-Ca@DOPA composites, a net neutral surfactant (i.e. DSPE-PEG_{2K}) was applied to allow such composites to suspend within an aqueous solution. Typically, 0.1 mL of the Zol-Ca@DOPA solution was added into a glass vial with 1 mg DSPE-PEG_{2K}, followed by the removal of $CHCl_3$. Thereafter, 1 mL IE-HPLC mobile phase (0.2% formic acid, pH ~3.0) was added into the glass vial and sonicated for several minutes. The concentration of Zol in the solution was then measured by IE-HPLC,

Besides Zol-Ca@DOPA, DOPA-coated alendronic acid-calcium (Ale-Ca@DOPA), clodronic acid-calcium (Clo-Ca@DOPA) and zoledronic acid-zinc (Zol-Zn@DOPA) complexes with spherical shape were also prepared in the same manner and characterized using TEM.

Preparation and characterization of Zol-Ca complex-incorporated lipid-based nanoparticles (i.e. Zol-Ca@bi-lipid NPs)

To prepare Zol-Ca@bi-lipid NPs, Zol-Ca@DOPA composites and DSPE-PEG_{2K} were mixed in 2 mL $CHCl_3$ to obtain a transparent solution. Thereafter, the solution was applied to a rotary evaporator under reduced pressure to remove $CHCl_3$ and obtain a thin film. The thin film was hydrated using 1 mL water (or 10 mM sodium phosphate buffer if needed) and sonicated for several minutes, followed by passing through a 0.45 μm PVDF filter and storing at 4 °C.

The morphology of Zol-Ca@bi-lipid NPs was characterized by TEM. To prepare the specimen, carbon-coated grids were pretreated by glow-discharge, and then each grid was covered by 5 μL of Zol-Ca@bi-lipid NPs solution. After dryness, the specimen was directly characterized or negatively stained using a 2% UA solution before observation. The hydrodynamic size and zeta potential of the nanoparticles were measured using a Nano Zetasizer (Malvern, Westborough, MA). To determine the content of Zol, Zol-Ca@bi-lipid NPs were lyophilized and dissolved in mobile phase before applying to IE-HPLC. The recovery efficiency (RE) was the weight ratio of the detected Zol in the nanoparticles

divided by the inputted Zol amount. The drug-loading efficiency (DLE) was the weight ratio of the detected Zol in nanoparticles divided by the weight of the lyophilized nanoparticles.

In vitro release of Zol from Zol-Ca@bi-lipid NPs

The release of Zol from the Zol-Ca@bi-lipid NPs was determined by placing the nanoparticles into a dialysis tube (MWCO, 50 KDa, Spectrum Laboratories, Inc., Rancho Dominguez, CA). Dialysis tubes that contained 0.6 mg of Zol, free or in Zol-Ca@bi-lipid NPs, in 1 mL of release medium were placed into 9 mL of release medium (i.e. 10 mM sodium phosphate buffer, pH 7.4) and incubated in a 37 °C shaker incubator. At pre-designed time points, 1 mL release medium was withdrawn and replaced with 1 mL fresh release medium. The concentration of Zol in the release medium was measured using IE-HPLC.

In vitro cellular cytotoxicity of Zol-Ca@bi-lipid NPs

A standard MTT assay was used to evaluate the cytotoxicity of Zol-Ca@bi-lipid NPs to the J774A.1 cells. Cells were seeded in 96-well plates (5×10^3 cells per well), followed by incubation for 24 h. Cells were then treated with free Zol, Zol-Ca@bi-lipid NPs, or a Zol-free DOPA liposome formulation as a control. The method of preparing the DOPA liposomes consisted of calcium-treated DOPA and DSPE-PEG_{2K} was almost the same as the method of preparing the Zol-Ca@bi-lipid NPs, except that an equivalent amount of calcium-treated DOPA instead of Zol-Ca@DOPA was used.

After 48 h of incubation at 37 °C, 20 μL of MTT solution (5 mg/mL in PBS) was added into the culture medium and incubated for 2 h. Thereafter, the culture medium was replaced by 150 μL of dimethyl sulfoxide. After 15 min of incubation, the absorbance at 570 nm in each well was measured using a Synergy HT microplate reader (BioTek, Winooski, VT). The 50% inhibitory concentration (IC_{50}) values were calculated using the GraphPad Prism (GraphPad Software, Inc., La Jolla, CA.).

Effect of Zol-Ca@bi-lipid NPs on the distribution of Zol in tumor tissues in a mouse model

The ability of the Zol-Ca@bi-lipid NPs in delivering Zol into tumors was evaluated in C57BL/6 mice with orthotopic M-Wnt mammary tumors (n = 4). Tumor-bearing mice were intravenously injected with Zol-Ca@bi-lipid NPs, free Zol, or PBS (as a control) 30 days after M-Wnt tumor cells (1×10^6) were injected into mice (average tumor diameter, ~8 nm). The dose of Zol was 2 μg per mouse, and 2% (w/w) of the Zol was AF647-labeled. Mice were euthanized 24 h later, and tumors were dissected and imaged using the IVIS Spectrum imaging system (Caliper Life Sciences, Waltham, MA) with excitation/emission wavelength of 640/680 nm..

In order to further confirm the modification of the biodistribution of Zol by Zol-Ca@bi-lipid NPs, the effect of the Zol-Ca@bi-lipid NPs on the population of TAMs in the tumors was evaluated. Mice with orthotopic M-Wnt mammary tumors were intravenously injected with Zol-Ca@bi-lipid NPs, free Zol, or PBS (as a control) 36 days after tumor cell injection (i.e. mean tumor diameter ~10 mm). Zol-free DOPA liposomes were also used as a vehicle control. The dose of Zol was 10 μg per mouse, and the injection was repeated two days later.

Forty-eight hours after the second injection, mice were euthanized to collect tumor tissues. To prepare single cell suspension, tumors were digested with 1 mg/mL of collagenase IV in Hank's Balanced Salt Solution (HBBS, Gibco) with 3 mM $CaCl_2$, followed by passing through a 70 μm strainer (Thermo Fisher Scientific) to collect cells. After washing with PBS twice, cells were fixed in 4% paraformaldehyde at room temperature for 30 min and then stained with APC-labeled anti-CD206 antibody on ice for 1 h. After washing with cold PBS twice, cells were analyzed using a BD FACS Aria Flow Cytometer (BD Biosciences-US, San Jose, CA) to determine the percent of $CD206^+$ cell (a biomarker of TAMs).[30]

Statistical analysis

Statistical analyses were accomplished using the Prism software. A p value of ≤ 0.05 is considered significant.

Results and Discussion

Effects of the component ratio of the RM on the properties of Zol-Ca complexes synthesized using the RM method

The RM system used for the synthesis of Zol-Ca complexes consisted of H_2O, NP-5 as the surfactant, and cyclohexane as the oil phase (denoted as RM_1). We first investigated the relationships between the physical properties of Zol-Ca complexes formed and the ratio of the different components in the RM_1. Shown in Figure 1 are representative TEM micrographs of Zol-Ca complexes synthesized in RM_1 with different $V_{H_2O}/V_{NP\text{-}5}$ and $V_{NP\text{-}5}/V_{cyclohexane}$ ratios. When the ratio of $V_{H_2O}/V_{NP\text{-}5}$ was fixed at 1/13.3, the Zol-Ca complexes formed were spherical and uniform in size, although the majority of the complexes existed as aggregates. Moreover, increasing the $V_{NP\text{-}5}/V_{cyclohexane}$ ratio from 9/91 to 35/75 led to an increase in the size of the complexes formed (i.e. from ~10 nm to ~20 nm), but did not show any significant effect on the spherical shape or the aggregation status of the complexes (Figure 1A).

When the ratio of $V_{H_2O}/V_{NP\text{-}5}$ was increased to 1/3 or higher, the as-synthesized Zol-Ca complexes exhibited pearl-necklace-like structures (i.e. connection or aggregation of different Zol-Ca complexes along certain directions). The whole length of the structures ranges from several tens to several hundreds of nanometers, and the diameter of the structural unit of such pearl-necklace-like complexes is ~8 nm (Figure 1C and 1D). Additionally, changing the $V_{NP\text{-}5}/V_{cyclohexane}$ ratio from 9/91 to 35/75 did not significantly influence the physical properties of Zol-Ca complexes formed (Figure 1D).

Taken together, these results indicate that the component ratio in the RM_1 system strongly influences the shape of resultant Zol-Ca complexes, and also slightly affect the size of spherical complexes but not the pearl-necklace-like complexes. The formation of spherical or pearl-necklace-like complexes is mainly determined by the ratio of the water/surfactant (i.e. $V_{H_2O}/V_{NP\text{-}5}$), and the size of the spherical Zol-Ca complexes is mainly affected by the ratio of surfactant/oil phase (i.e. $V_{NP\text{-}5}/V_{cyclohexane}$). A ternary phase diagram was plotted to illustrate the relationships between the morphology (i.e. shape and size) of Zol-Ca complexes synthesized and the compositions of the RM_1 (Figure 2). Since the $V_{NP\text{-}5}$/

$V_{cyclohexane}$ ratio did not significantly affect the shape of Zol-Ca complexes formed, the RM system with a fixed $V_{NP\text{-}5}/V_{cyclohexane}$ ratio of 30/70 was selected for further studies.

Effects of co-surfactant(s) on the properties of Zol-Ca complexes synthesized using the RM method

We then investigated the effect of including co-surfactant(s) in the RM_1 system on the properties of Zol-Ca complexes synthesized. It was verified that the inclusion of OEP-10 or hexanol as a co-surfactant led to an increase in the size of the spherical Zol-Ca complexes formed (Figure S1), as compared to the complexes formed in RM_1 without any co-surfactant (Figure 1A-3). Due to the poor solubility of OEP-10 in cyclohexane and the difficulty in forming transparent hexanol-containing RM with high concentrations of $CaCl_2$ solution, a combined co-surfactant system (i.e. $V_{OEP\text{-}10}/V_{hexanol}$ ratio fixed at 2/1) was selected, and the RM that contains such combined co-surfactant system are named as RM_2. Shown in Figure 3A are representative TEM micrographs of the Zol-Ca complexes synthesized in RM_2 with fixed $V_{H_2O}/V_{total\ surfactants}$ and $V_{total\ surfactants}/V_{cyclohexane}$ ratios of 1/13.3 and 30/70, respectively, which is identical to that in RM_1, except that a portion of NP-5 (i.e. 25% to 100%) was replaced with the combined co-surfactant system (i.e. $V_{NP\text{-}5}/V_{OEP\text{-}10\ +\ hexanol}$ ratios of 75:25, 50:50, 25:75 or 0:100). When the $V_{NP\text{-}5}/V_{OEP\text{-}10\ +\ hexanol}$ ratio was 75/25, the Zol-Ca complexes formed were still spherical, and their size, ranging from 25 to 80 nm, was significantly increased, as compared to complexes formed in the RM without any co-surfactant (Figure 3A-1, versus Figure 1A-3). When the $V_{NP\text{-}5}/V_{OEP\text{-}10\ +\ hexanol}$ ratio was decreased (e.g. from 75/25 to 50/50 or 25/50), the resultant complexes remained mainly spherical, but the particle sizes are not uniform, and non-spherical or irregular shape products were also formed (Figure 3A-2 and 3A-3, indicated by white arrows). Without NP-5 (i.e. $V_{NP\text{-}5}/V_{OEP\text{-}10\ +\ hexanol}$ ratio of 0/100) in RM_2, spherical particles were rarely formed, and the resultant products were mainly irregular bulk materials (Figure 3A-4).

We also investigated the effect of the co-surfactants on the properties of the pearl-necklace-like complexes. Shown in Figure 3B are typical TEM micrographs of the pearl-necklace-like Zol-Ca complexes formed in RM_2 with fixed $V_{H_2O}/V_{total\ surfactants}$ and $V_{total\ surfactants}/V_{cyclohexane}$ ratios of 1/1.5 and 30/70, respectively (the same component ratio to that shown in Figure 1D-3), and $V_{NP\text{-}5}/V_{OEP\text{-}10\ +\ hexanol}$ ratios varying from 75:25 to 0:100. It appeared that the inclusion of co-surfactants had no significant influence on the pearl-necklace-like structures, but resulted in the formation of additional irregular products.

These results indicate that certain percentages of co-surfactants in the RM can increase the size of the resultant spherical Zol-Ca complexes, but did not significantly affect the physical properties of pearl-necklace-like complexes. Moreover, it may induce the generation of irregular bulk materials. A ternary phase diagram was drawn to describe the change in the morphology of the Zol-Ca complexes formed as a result of the addition of co-surfactants (Figure 4).

Effects of reaction time, reactant concentration, and reaction temperature on the properties of Zol-Ca complexes synthesized

In following experiments, we investigated whether the physical properties of Zol-Ca complexes synthesized are influenced by other conditions such as reaction time, the concentration of reactants in RM, or the reaction temperature. For the spherical Zol-Ca complexes, shown in Figure S2A are representative TEM micrographs of Zol-Ca complexes prepared in RM after reaction for different time periods. Compared to an overnight reaction (i.e. ~16 h of reaction, Figure 1A-3), the Zol-Ca complexes formed after 0.5 h of reaction are smaller (Figure S2A-1), whereas the Zol-Ca complexes formed after 4 h and 44 h of reaction are similar to those formed after ~16 h of reaction with respect to morphology, size and aggregation statues (Figure S2A-2 and S2A-3). These results indicated that the reaction of the formation of the spherical Zol-Ca complexes required at least 4 h to reach equilibrium.

Shown in Figure 5A are representative TEM micrographs of Zol-Ca complexes formed in RM_1 with different concentrations of $CaCl_2$ or Zol. When the concentration ratio of $CaCl_2$/Zol was fixed at 7.5/1, increasing their concentrations from 0.15 M/0.02 M (used for the sample in Figure 1A-3) to 0.375 M/0.05 M and 0.6 M/0.08 M did not affect the physical properties of Zol-Ca complexes formed (Figure 5A-1 and 5A-2). On the other hand, when the concentration of $CaCl_2$ was fixed at 0.15 M, increasing the concentration of Zol from 0.02 M (used for sample in Figure 1A-3) to 0.05M and 0.08 M led to the formation of slightly smaller Zol-Ca complexes (Figure 5A-3 and 5A-4).

Shown in Figure 5B are representative TEM micrographs of Zol-Ca complexes synthesized at ~30 °C and ~10 °C. Compared to that formed under ~22 °C (see Figure 1A-3), it seemed that the reaction temperature did not significantly affect the shape, size or aggregation status of the Zol-Ca complexes synthesized.

Compared to the formation of spherical Zol-Ca complexes, insufficient reaction time (i.e. 0.5 h) could result in the formation of slightly thinner pearl-necklace-like Zol-Ca complexes, and it appears that the reaction also required at least 4 h to reach equilibrium (Figure S2B). Moreover, the physical properties of pearl-necklace-like Zol-Ca complexes are not significantly influenced by the reactant concentration or reaction temperature (data not shown). Based on these results, it is concluded that the reactant concentration and reaction temperature are not the primary determinants of the physical properties of Zol-Ca complexes synthesized.

Effect of DOPA on the properties of Zol-Ca complexes synthesized using the RM method

Next, we evaluated the effect of adding DOPA, an anionic phospholipid, into the RM on the physical properties of resultant Zol-Ca complexes, because it was reported that DOPA can help minimize the aggregation status and enhance relative monodispersity of nanoparticles synthesized by RM method.[31] We first investigated the effect of DOPA on the physical properties of Zol-Ca complexes prepared in the RM_1 system. DOPA (with a final concentration of 0.45 mM) was added into the RM before the initiation of reaction between $CaCl_2$ and Zol. As shown in Figure 6A-1, when the $V_{H_2O}/V_{NP\text{-}5}$ ratio in the DOPA-containing RM_1 was 1/13.3, the edge of the spherical Zol-Ca complexes formed and the

space between these complexes can be readily observed, indicating an improved monodispersity of such complexes, as compared to those prepared without DOPA (Figure 1A-3). When the $V_{H_2O}/V_{NP\text{-}5}$ ratio in the DOPA-containing RM_1 was increased from 1:13.3 to 1/3 or 1/1.5, the final products synthesized only contained abundant small irregular particulates with good monodispersity and uniformity, but the pearl-necklace-like structures disappeared (Figure 6A-3 or 6A-4, versus Figure 1D-3). This suggests that the presence of DOPA in the RM_1 prevents the formation of pearl-necklace-like structures.

We then studied whether changing the time point at which DOPA is added into the RM influences the physical properties of Zol-Ca complexes synthesized. In this case, DOPA (with a final concentration of 0.45 mM) was added into the RM_1 system 4 h after the initiation of reaction between $CaCl_2$ and Zol. As shown in Figure 6B-1, when the $V_{H_2O}/V_{NP\text{-}5}$ ratio was 1/13.3, the shape, size, uniformity and monodispersity of resultant Zol-Ca complexes were very similar to that shown in Figure 6A-1, indicating that changing the time point at which DOPA is added does not significantly affect the physical properties of spherical Zol-Ca complexes. In contrast, when the $V_{H_2O}/V_{NP\text{-}5}$ ratio was 1/1.5, the final complexes formed were short necklace-like (Figure 6B-2, white arrows); indicating that adding DOPA into the RM after the initiation of the reaction in the RM system may weaken its influence on the morphology of pear-necklace-like Zol-Ca complexes.

Considering that DOPA was capable of minimizing the aggregation of spherical Zol-Ca complexes prepared in the RM_1 system, we then investigated whether it has a similar effect on spherical Zol-Ca complexes synthesized in the co-surfactant-containing RM_2 system. As shown in Figure 6C-1 and 6C-2, when the $V_{NP\text{-}5}/V_{OEP\text{-}10\ +\ hexanol}$ ratio in RM_2 with 0.45 mM DOPA were 75/25 and 50/50, respectively, the Zol-Ca complexes formed also showed good monodispersity, although remained non-uniform. When the $V_{NP\text{-}5}/V_{OEP\text{-}10\ +\ hexanol}$ ratio was decreased to 0/100 (i.e. without NP-5), there were more spherical Zol-Ca complexes and much less irregular shape products, as compared to that prepared in the RM_2 without DOPA (Figure 6C-4 versus Figure 3A-4), indicating that DOPA may facilitate the formation of regular spherical shape in RM_2 system.

The above results demonstrated that the presence of DOPA in the RM can significantly improve the monodispersity of the resultant spherical or small irregular Zol-Ca complexes. This is likely because the phosphate group in DOPA interacts with the calcium cations on the surface of the Zol-Ca complexes, and thus leading to the formation of a protective layer that helps to reduce the aggregation of the complexes.[31] Additionally, it is noting that such DOPA layer also changes the Zol-Ca complexes from hydrophilic to hydrophobic. The aforementioned Zol-Ca complexes without DOPA-coating can be easily suspended in water or polar solvent such as ethanol. However, the DOPA-coated Zol-Ca complexes are insoluble in water and can only be suspended in non-polar solvent such as $CHCl_3$. This change in hydrophilicity/hydrophobicity further demonstrated the versatility of the RM-based synthesis methodology in controlling the physical properties of (bis)phosphonate-metal complexes.

Proposed mechanisms of the formation of Zol-Ca complexes of various physical properties in the RM

Data presented above clearly showed that the Zol-Ca complexes with various physical properties (e.g. shape, size, uniformity, dispersity and hydrophilicity) can be controllably synthesized by using the RM method. It is well known that the morphology of nanoparticulate products synthesized by the RM method is tightly related to the shape of inner water phase of the RM system.[17–18] Usually, a typical RM that contains a small amount of water has isolated spherical inner water phase (i.e. water droplets in oil phase) (Figure 7A-1); when the amount of water is increased, the typical RM may undergo a transition to become a bicontinuous RM (or oil-rich bicontinuous microemulsion), which has a zig-zag channel-like water phase (Figure 7A-2).[16, 18] For the NP-5-based RM system, it has been reported that the channel-like water phase forms when the molar ratio of H_2O/NP-5 is over 10, equivalent to a $V_{H_2O}/V_{NP\text{-}5}$ ratio of 1/2.5.[32–33]

In RM with isolated spherical water droplets, it is mostly accepted that the reaction occurs when the reactant-containing droplets collide with each other.[17–18] In our study, such collisions enable the exchange of reactants (i.e. $CaCl_2$ and Zol) in different RM droplets (Figure 7B, the scheme with green arrows), thereby resulting in the formation of spherical Zol-Ca complexes. After the reaction, the RM system was broken using ethanol and the complexes obtained were collected by high speed centrifugation, washed, and then re-suspended. Aggregation of these bare Zol-Ca complexes may occur during any of these steps (e.g. Figure 1A). In contrast, when DOPA was included in the synthesis process (Figure 7B, scheme with purple arrows), the aggregation of the Zol-Ca complexes was minimized (e.g. Figure 6A-1), likely because DOPA molecules bound to the surface of Zol-Ca complexes and formed a protective layer. Interestingly, when DOPA was added into the RM system 4 h after the initiation of the reaction between $CaCl_2$ and Zol, the Zol-Ca complexes obtained still possessed excellent monodispersity (Figure 6B-1). These findings indicated that the aggregation of Zol-Ca complexes likely occurred after the breakage of RM (by the addition of ethanol), because if Zol-Ca complexes already aggregated together during the reaction step, it is not expected that the addition of DOPA after the initiation of the reaction will be able to prevent such aggregation.

The size of spherical droplets in nonionic surfactant-containing RM usually relies on the chain length of the hydrophilic moiety of the surfactant (e.g. the PEG chains in NP-5 and OEP-10).[34] Since the PEG chain of OEP-10 is about two-fold longer than that of NP-5, the addition of OEP-10 into the RM with NP-5 can induce the formation of large droplets. In addition, hexanol, a medium chain-length alcohol, is known to assist primary surfactants to decrease the interfacial tension and allow the formation of large droplets.[17] Therefore, it is not surprising that the Zol-Ca complexes formed in RM_2 with the combined co-surfactant system of OEP-10 and hexanol are larger than those formed in the same RM system without the co-surfactants (i.e. RM_1) (Figure 3A-1 versus 1A-3, or 6C-1 versus 6A-1).

Compared to the typical RM, the bicontinuous RM is more complicated and it remains unknown about the details of the reactions occurring in such RM system. Nevertheless, since the morphology of complexes formed mainly dependents on the structure of water phase in the RM as mentioned above, the formation of the pearl-necklace-like Zol-Ca complexes may

be related to the zig-zag channel-like water phase in the bicontinuous RM. As shown in Figure 7C (the scheme with green arrows), although the manner by which the reactants exchanged is unclear, small Zol-Ca complexes were still generated. These small complexes may move freely to connect (or aggregate) with each other to form the pearl-necklace-like complexes, due to the continuous nature of the inner zig-zag channel-like water phase in RM. Compared to this, when DOPA was added into Zol-containing RM before the initiation of reaction (Figure 7C, the scheme with purple arrows), the surface of Zol-Ca complexes may have been occupied by DOPA molecules during the reaction step, which prevented further connection (or aggregation) between those complexes. This explains the small size and good monodispersity of the final irregular particulates shown in Figure 6A-4. Moreover, when DOPA was added into the RM system 4 h after the initiation of the reaction, the final products were short necklace-like (Figure 6B-2). This may be attributed to that the connection (or aggregation) of Zol-Ca complexes has already occurred before the addition of DOPA, thus indirectly verifying that the formation of pearl-necklace-like Zol-Ca complexes is likely related to the connection (or aggregation) of the small irregular Zol-Ca complexes formed in the bicontinuous RM. However, more experiments need to be carried out to fully elucidate the mechanisms underlying the formation of pearl-necklace-like structures.

Evaluation of the potential application of the Zol-Ca complexes synthesized by the RM method: enhancement of the distribution of Zol in tumor tissues in a mouse model with orthotopic mammary tumor

It was reported that reformulating Zol to Zol-loaded liposomes or nanoparticles can help increase the accumulation of Zol in extraskeletal tumors and improve the relevant therapeutic effect.[35–43] The RM technique allows us to synthesize a variety of Zol-Ca complexes with controlled physical properties. To preliminarily evaluate the potential biomedical application of the as-synthesized Zol-Ca complexes, we sought to formulate one of the many types of the Zol-Ca complexes synthesized into lipid-based nanoparticles and tested the feasibility of using the resultant nanoparticle formulation for enhanced delivery of Zol into extraskeletal tumors. Although there are reports that non-spherical nanomaterials (e.g. filament-like,[44] rod-like,[45] etc.) show unique characteristics in drug delivery, particulate materials with regular spherical shape, uniform size around 20–200 nm and good monodispersity are more commonly used.[46–47] Therefore, a hydrophobic DOPA-coated Zol-Ca complexes with spherical shape, uniform size of ~15 nm and excellent monodispersity (Figure 6A-1, denoted as Zol-Ca@DOPA) were chosen and combined with DSPE-PEG_{2K}, a PEGylated phospholipid, to form a lipid-based Zol-Ca@DOPA nanoparticle formulation (i.e. Zol-Ca@bi-lipid NPs). It is assumed that the Zol-Ca complexes were wrapped by a mixed lipid layer consisted of DOPA and DSPE-PEG_{2K} (Figure S3A). After optimization (data not shown), the Zol-Ca@bi-lipid NPs prepared with a weight ratio of 20 μg Zol to 1 mg DSPE-PEG_{2K} (RE and DLE of 78.3 ± 1.2% and 2.4 ± 0.2%, respectively) was selected for further characterization and in vivo studies. TEM showed that the Zol-Ca@bi-lipid NPs were spherical, uniform and monodispersed (Figure S3B). Further negative staining verified that such nanoparticles appear to have a ‘core-shell’ structure as mentioned above (Figure 8A, white arrows). The mean hydrodynamic diameter and zeta potential of Zol-Ca@bi-lipid NPs in aqueous suspension were 23.6 ± 1.8 nm and −32.2 ± 3.5 mV, respectively. Under physiological pH, 40–45% of Zol was released from the Zol-Ca@bi-lipid NPs after 48 h of

incubation at 37 °C (Figure S4). Moreover, cell cytotoxicity study indicated that Zol-Ca@bi-lipid NPs were more potent than free Zol in inhibiting the proliferation of murine J774A.1 macrophages (Figure 8B, IC_{50} value of ~4.6 μM versus ~26.8 μM).

In order to readily detect Zol in tumors, the Zol-Ca@bi-lipid NPs were prepared with Zol that contained 2% (w/w) of AF647-labeled Zol (i.e. Zol-AF647). The fluorescently labeled bisphosphonates such as Zol-AF647 have been used by other groups to study the biodistribution of bisphosphonates in animal models.[48–50] As shown in Figure 8C, in a mouse model with orthotopic M-Wnt mammary tumors, 24 h after i.v. injection, the content of Zol in tumors in the group of mice injected with the Zol-Ca@bi-lipid NPs was about 9.3-fold higher than that in the group of mice injected with free Zol (fluorescent images are shown in Figure S5). Although the data obtained using the Zol-AF647 may not be exactly the same as using unlabeled Zol, it is clear that the formulation of the Zol or Zol-AF647 into the Zol-Ca@bi-lipid NPs increases its accumulation in tumors. In fact, such modification of the distribution of the Zol by the Zol-Ca@bi-lipid NPs was also indirectly confirmed by the improved effect of Zol-Ca@bi-lipid NPs, relative to the equivalent dose of free Zol, in reducing the population of $CD206^+$ TAMs in the mouse model with M-Wnt tumors (Figure 8D).

Recently, there is increasing interest in developing new bisphosphonate formulations to better exploit their biomedical applications. Au et al. prepared spherical bisphosphonate-metal particles based on the RM method and coated such particles with folic acid-modified lipids for target delivery of Zol into tumors to kill tumor cells, but they did not systematically study the effect of RM conditions on the physical properties of the resultant bisphosphonate-metal material or the influence of their formulation on TAMs in tumors.[21] Besides the formulations (including our own) prepared with pre-synthesized bisphosphonate-metal materials, others have reported the development of bisphosphonate-loaded organic, inorganic or organic/inorganic hybrid nanoparticles for cancer treatments. For instance, bisphosphonates (e.g. Zol or Clo) have been directly encapsulated into liposomes to increase their concentrations in tumors.[35–37] Risedronic acid has been loaded into metal cation-functionalized mesoporous silica nanoparticles to reduce its release rate from the mesoporous silica, thus improving its inhibitory effect against tumor cells in culture.[51] Zol was also complexed with pre-formed calcium phosphate nanoparticles/complexes and then encapsulated into liposomes and nanoparticles, and those formulations were also found to enhance the accumulation of Zol in tumors.[38–43] Moreover, a similar fomulation has also been applied to co-deliver Zol and double-stranded RNA into tumors.[52]

Finally, although the above preliminary studies only demonstrated that the biomedical application of the hydrophobic, spherical Zol-Ca@DOPA composites of ~15 nm, other Zol-Ca complexes synthesized by the RM method such as the ones with the pearl-necklace-like structures (Figure 1D-3), the ones that are non-spherical but uniformly distributed (Figure 6A-4), the ones with spherical shapes and non-uniform large sizes (Figure 6C-1), or any Zol-Ca complexes coated with another lipid other than DOPA, may also have other application potentials, and we are currently evaluating them in our lab. Moreover, it is worth pointing out that such RM-based synthesis approach is not limited to the preparation of Zol-Ca complexes only. Other bisphosphonate-metal complexes, such as DOPA-coated alendronic

acid-calcium (Ale-Ca), clodronic acid-calcium (Clo-Ca) and zoledronic acid-zinc (Zol-Zn) (Figure S6), were also successfully prepared by the same method. In this regard, the robust RM-based approach of synthesizing (bis)phosphonate-metal materials is expected to expand and improve their industrial and biomedical applications. Furthermore, data from a preliminary study showed that the molar ratios of Ca to Zol in the Zol-Ca complexes synthesized are significantly different when the RM conditions are changed (e.g. V_{H_2O}/$V_{cyclohexane}$ ratio, presence of DOPA) (Table S1), indicating that the chemical compositions (or relative molecular structure, crystallinity, etc.) of different Zol-Ca complexes may also be different. More experiments will need to be carried out to understand the relationship between the RM condition parameters and the chemical compositions of resultant Zol-Ca complexes.

Conclusion

In the present study, we comprehensively studied RM-based synthesis of (bis)phosphonate-metal materials using Zol-Ca complexes as examples and explained the mechanism(s) underlying the relationship between the physical properties of the Zol-Ca complexes synthesized and various parameters of RM system, such as the composition ratio in RM, co-surfactant, reactant concentrations, reaction temperature, and the presence of DOPA. The main determinant of the morphology of Zol-Ca complexes (i.e. spherical or pearl-necklace-like structures) is the component ratio of water/surfactant in the RM. The addition of co-surfactants in the RM significantly increases the size, but reduces the uniformity of the spherical Zol-Ca complexes, while having no significant effect on the pearl-necklace-like structures. Reactant concentrations slightly affect the size of the spherical complexes, whereas reaction temperature does not have any significant effect. The presence of DOPA in the reaction improves the monodispersity of spherical Zol-Ca complexes, but breaks the pearl-necklace-like structures. Finally, using one of the Zol-Ca complexes coated with DOPA (i.e. Zol-Ca@DOPA), we provided evidence that formulating the Zol-Ca complexes into lipid-based nanoparticles (~24 nm) can improve the delivery of Zol in tumors in a mouse model. The controlled synthesis of (bis)phosphonate-metal complexes with desirable physical properties is expected to expand their potential biomedical applications.

Supplementary Material

Refer to Web version on PubMed Central for supplementary material.

Acknowledgments

This work was supported in part by a National Institutes of Health grant (CA135274 to Z.C.). Solange Valdes is a winner of the Becas-Chile Scholarship from the Government of Chile.

References

1. Clearfield, A., Demadis, K. Metal Phosphonate Chemistry: From Synthesis to Applications. Royal Society of Chemistry; 2011.
2. Alberti G, Costantino U, Allulli S, Tomassini N. Crystalline Zr (R-PO_3)$_2$ and Zr (R-OPO_3)$_2$ Compounds (R= Organic Radical): A New Class of Materials Having Layered Structure of the Zirconium Phosphate Type. J Inorg Nucl Chem. 1978; 40:1113–1117.

3. Alkordi MH, Liu Y, Larsen RW, Eubank JF, Eddaoudi M. Zeolite-Like Metal-Organic Frameworks as Platforms for Applications: On Metalloporphyrin-Based Catalysts. J Am Chem Soc. 2008; 130:12639–12641. [PubMed: 18759392]
4. García EJ, Mowat JP, Wright PA, Pérez-Pellitero J, Jallut C, Pirngruber GD. Role of Structure and Chemistry in Controlling Separations of CO_2/CH_4 and $CO_2/CH_4/CO$ Mixtures over Honeycomb Mofs with Coordinatively Unsaturated Metal Sites. J Phys Chem C. 2012; 116:26636–26648.
5. Shimizu GK, Taylor JM, Kim S. Proton Conduction with Metal-Organic Frameworks. Science. 2013; 341:354–355. [PubMed: 23888028]
6. Amalric J, Mutin PH, Guerrero G, Ponche A, Sotto A, Lavigne JP. Phosphonate Monolayers Functionalized by Silver Thiolate Species as Antibacterial Nanocoatings on Titanium and Stainless Steel. J Mater Chem. 2009; 19:141–149.
7. Beutner R, Michael J, Schwenzer B, Scharnweber D. Biological Nano-Functionalization of Titanium-Based Biomaterial Surfaces: A Flexible Toolbox. J R Soc, interface. 2010; 7:S93–S105. [PubMed: 19889692]
8. Clearfield A. Recent Advances in Metal Phosphonate Chemistry Ii. Curr Opin Solid State Mater Sci. 2002; 6:495–506.
9. Shimizu GK, Vaidhyanathan R, Taylor JM. Phosphonate and Sulfonate Metal Organic Frameworks. Chem Soc Rev. 2009; 38:1430–1449. [PubMed: 19384446]
10. Maeda K. Metal Phosphonate Open-Framework Materials. Microporous Mesoporous Mater. 2004; 73:47–55.
11. Nicole L, Boissière C, Grosso D, Quach A, Sanchez C. Mesostructured Hybrid Organic-Inorganic Thin Films. J Mater Chem. 2005; 15:3598–3627.
12. Zhu YP, Ma TY, Liu YL, Ren TZ, Yuan ZY. Metal Phosphonate Hybrid Materials: From Densely Layered to Hierarchically Nanoporous Structures. Inorg Chem Front. 2014; 1:360–383.
13. El Haskouri J, Guillem C, Latorre J, Beltrán A, Beltrán D, Amorós P. The First Pure Mesoporous Aluminium Phosphonates and Diphosphonates - New Hybrid Porous Materials. Eur J Inorg Chem. 2004; 2004:1804–1807.
14. Alberti G, Marmottini F, Vivani R, Zappelli P. Preparation and Characterization of Pillared Zirconium Phosphite-Diphosphonates with Tuneable Inter-Crystal Mesoporosity. J Porous Mater. 1998; 5:221–226.
15. Kimura T. Synthesis of Mesostructured and Mesoporous Aluminum Organophosphonates Prepared by Using Diphosphonic Acids with Alkylene Groups. Chem Mater. 2005; 17:337–344.
16. Pileni MP. The Role of Soft Colloidal Templates in Controlling the Size and Shape of Inorganic Nanocrystals. Nat Mater. 2003; 2:145–150. [PubMed: 12612669]
17. Malik MA, Wani MY, Hashim MA. Microemulsion Method: A Novel Route to Synthesize Organic and Inorganic Nanomaterials: 1st Nano Update. Arabian J Chem. 2012; 5:397–417.
18. Tovstun SA, Razumov VF. Preparation of Nanoparticles in Reverse Microemulsions. Russ Chem Rev. 2011; 80:953–969.
19. He C, Liu D, Lin W. Self-Assembled Nanoscale Coordination Polymers Carrying Sirnas and Cisplatin for Effective Treatment of Resistant Ovarian Cancer. Biomaterials. 2015; 36:124–133. [PubMed: 25315138]
20. Liu D, Poon C, Lu K, He C, Lin W. Self-Assembled Nanoscale Coordination Polymers with Trigger Release Properties for Effective Anticancer Therapy. Nat Commun. 2014; 5:4182–4193. [PubMed: 24964370]
21. Au KM, Satterlee A, Min Y, Tian X, Kim YS, Caster JM, Zhang L, Zhang T, Huang L, Wang AZ. Folate-Targeted PH-Responsive Calcium Zoledronate Nanoscale Metal-Organic Frameworks: Turning a Bone Antiresorptive Agent into an Anticancer Therapeutic. Biomaterials. 2016; 82:178–193. [PubMed: 26763733]
22. Kubista B, Trieb K, Sevelda F, Toma C, Arrich F, Heffeter P, Elbling L, Sutterlüty H, Scotlandi K, Kotz R. Anticancer Effects of Zoledronic Acid against Human Osteosarcoma Cells. J Orthop Res. 2006; 24:1145–1152. [PubMed: 16602111]
23. Coleman R, Gnant M, Morgan G, Clezardin P. Effects of Bone-Targeted Agents on Cancer Progression and Mortality. J Natl Cancer Inst. 2012; 104:1059–1067. [PubMed: 22752060]

24. Marra M, Abbruzzese A, Addeo R, Prete S, Tassone P, Tonini G, Tagliaferri P, Santini D, Caraglia M. Cutting the Limits of Aminobisphosphonates: New Strategies for the Potentiation of Their Anti-Tumour Effects. Curr Cancer Drug Targets. 2009; 9:791–800. [PubMed: 20025567]
25. Brown JE, Neville-Webbe H, Coleman RE. The Role of Bisphosphonates in Breast and Prostate Cancers. Endocr -Relat Cancer. 2004; 11:207–224. [PubMed: 15163299]
26. Rosen LS, Gordon D, Tchekmedyian S, Yanagihara R, Hirsh V, Krzakowski M, Pawlicki M, de Souza P, Zheng M, Urbanowitz G. Zoledronic Acid Versus Placebo in the Treatment of Skeletal Metastases in Patients with Lung Cancer and Other Solid Tumors: A Phase III, Double-Blind, Randomized Trial--the Zoledronic Acid Lung Cancer and Other Solid Tumors Study Group. J Clin Oncol. 2003; 21:3150–3157. [PubMed: 12915606]
27. Rosen LS, Gordon D, Tchekmedyian NS, Yanagihara R, Hirsh V, Krzakowski M, Pawlicki M, De Souza P, Zheng M, Urbanowitz G. Long-Term Efficacy and Safety of Zoledronic Acid in the Treatment of Skeletal Metastases in Patients with Nonsmall Cell Lung Carcinoma and Other Solid Tumors. Cancer. 2004; 100:2613–2621. [PubMed: 15197804]
28. Niu M, Valdes S, Naguib YW, Hursting SD, Cui Z. Tumor-Associated Macrophage-Mediated Targeted Therapy of Triple-Negative Breast Cancer. Mol Pharmaceutics. 2016; 13:1833–1842.
29. Raghu NS. A New Analytical Method for Estimation of Zoledronic Acid in Commercial Pharmaceutical Injections by Ion-Exchange (IEC) High Performance Liquid Chromatography. J Liq Chromatogr Relat Technol. 2011; 34:476–489.
30. Roca H, Varsos ZS, Sud S, Craig MJ, Ying C, Pienta KJ. CCL2 and Interleukin-6 Promote Survival of Human Cd11b+ Peripheral Blood Mononuclear Cells and Induce M2-Type Macrophage Polarization. J Biol Chem. 2009; 284:34342–34354. [PubMed: 19833726]
31. Li J, Yang Y, Huang L. Calcium Phosphate Nanoparticles with an Asymmetric Lipid Bilayer Coating for Sirna Delivery to the Tumor. J Controlled Release. 2012; 158:108–114.
32. Chang CL, Fogler HS. Controlled Formation of Silica Particles from Tetraethyl Orthosilicate in Nonionic Water-in-Oil Microemulsions. Langmuir. 1997; 13:3295–3307.
33. Bagwe RP, Yang C, Hilliard LR, Tan W. Optimization of Dye-Doped Silica Nanoparticles Prepared Using a Reverse Microemulsion Method. Langmuir. 2004; 20:8336–8342. [PubMed: 15350111]
34. Lawrence MJ, Rees GD. Microemulsion-Based Media as Novel Drug Delivery Systems. Adv Drug Delivery Rev. 2000; 45:89–121.
35. Zeisberger S, Odermatt B, Marty C, Zehnder-Fjällman A, Ballmer-Hofer K, Schwendener R. Clodronate-Liposome-Mediated Depletion of Tumour-Associated Macrophages: A New and Highly Effective Antiangiogenic Therapy Approach. Br J Cancer. 2006; 95:272–281. [PubMed: 16832418]
36. Marra M, Salzano G, Leonetti C, Tassone P, Scarsella M, Zappavigna S, Calimeri T, Franco R, Liguori G, Cigliana G. Nanotechnologies to Use Bisphosphonates as Potent Anticancer Agents: The Effects of Zoledronic Acid Encapsulated into Liposomes. Nanomedicine (N Y, NY, U S). 2011; 7:955–964.
37. Shmeeda H, Amitay Y, Tzemach D, Gorin J, Gabizon A. Liposome Encapsulation of Zoledronic Acid Results in Major Changes in Tissue Distribution and Increase in Toxicity. J Controlled Release. 2013; 167:265–275.
38. Salzano G, Marra M, Porru M, Zappavigna S, Abbruzzese A, La Rotonda M, Leonetti C, Caraglia M, De Rosa G. Self-Assembly Nanoparticles for the Delivery of Bisphosphonates into Tumors. Int J Pharm (Amsterdam, Neth). 2011; 403:292–297.
39. Marra M, Salzano G, Leonetti C, Porru M, Franco R, Zappavigna S, Liguori G, Botti G, Chieffi P, Lamberti M. New Self-Assembly Nanoparticles and Stealth Liposomes for the Delivery of Zoledronic Acid: A Comparative Study. Biotechnol Adv. 2012; 30:302–309. [PubMed: 21741464]
40. Salzano G, Zappavigna S, Luce A, D'Onofrio N, Balestrieri M, Grimaldi A, Lusa S, Ingrosso D, Artuso S, Porru M. Transferrin-Targeted Nanoparticles Containing Zoledronic Acid as a Potential Tool to Inhibit Glioblastoma Growth. J Biomed Nanotechnol. 2016; 12:811–830. [PubMed: 27301207]
41. Kopecka J, Porto S, Lusa S, Gazzano E, Salzano G, Pinzòn-Daza ML, Giordano A, Desiderio V, Ghigo D, De Rosa G. Zoledronic Acid-Encapsulating Self-Assembling Nanoparticles and

Doxorubicin: A Combinatorial Approach to Overcome Simultaneously Chemoresistance and Immunoresistance in Breast Tumors. Oncotarget. 2016; 7:20753–20772. [PubMed: 26980746]

42. Schiraldi C, Zappavigna S, D'Agostino A, Porto S, Gaito O, Lusa S, Lamberti M, De Rosa M, De Rosa G, Caraglia M. Nanoparticles for the Delivery of Zoledronic Acid to Prostate Cancer Cells: A Comparative Analysis through Time Lapse Video-Microscopy Technique. Cancer Biol Ther. 2014; 15:1524–1532. [PubMed: 25482949]
43. Porru M, Zappavigna S, Salzano G, Luce A, Stoppacciaro A, Balestrieri ML, Artuso S, Lusa S, De Rosa G, Leonetti C. Medical Treatment of Orthotopic Glioblastoma with Transferrin-Conjugated Nanoparticles Encapsulating Zoledronic Acid. Oncotarget. 2014; 5:10446–10459. [PubMed: 25431953]
44. Geng Y, Dalhaimer P, Cai S, Tsai R, Tewari M, Minko T, Discher DE. Shape Effects of Filaments Versus Spherical Particles in Flow and Drug Delivery. Nat Nanotechnol. 2007; 2:249–255. [PubMed: 18654271]
45. Huang X, Li L, Liu T, Hao N, Liu H, Chen D, Tang F. The Shape Effect of Mesoporous Silica Nanoparticles on Biodistribution, Clearance, and Biocompatibility in Vivo. ACS nano. 2011; 5:5390–5399. [PubMed: 21634407]
46. Elsabahy M, Wooley KL. Design of Polymeric Nanoparticles for Biomedical Delivery Applications. Chem Soc Rev. 2012; 41:2545–2561. [PubMed: 22334259]
47. Park JH, Gu L, Von Maltzahn G, Ruoslahti E, Bhatia SN, Sailor MJ. Biodegradable Luminescent Porous Silicon Nanoparticles for in Vivo Applications. Nat Mater. 2009; 8:331–336. [PubMed: 19234444]
48. Junankar S, Shay G, Jurczyluk J, Ali N, Down J, Pocock N, Parker A, Nguyen A, Sun S, Kashemirov B. Real-Time Intravital Imaging Establishes Tumor-Associated Macrophages as the Extraskeletal Target of Bisphosphonate Action in Cancer. Cancer Discovery. 2015; 5:35–42. [PubMed: 25312016]
49. Roelofs AJ, Stewart CA, Sun S, Błażewska KM, Kashemirov BA, McKenna CE, Russell RGG, Rogers MJ, Lundy MW, Ebetino FH. Influence of Bone Affinity on the Skeletal Distribution of Fluorescently Labeled Bisphosphonates in Vivo. J Bone Miner Res. 2012; 27:835–847. [PubMed: 22228189]
50. Sun S, Błażewska KM, Kadina AP, Kashemirov BA, Duan X, Triffitt JT, Dunford JE, Russell RGG, Ebetino FH, Roelofs AJ. Fluorescent Bisphosphonate and Carboxyphosphonate Probes: A Versatile Imaging Toolkit for Applications in Bone Biology and Biomedicine. Bioconjugate Chem. 2015; 27:329–340.
51. Gu J, Huang M, Liu J, Li Y, Zhao W, Shi J. Calcium Doped Mesoporous Silica Nanoparticles as Efficient Alendronate Delivery Vehicles. New J Chem. 2012; 36:1717–1720.
52. Chen L, Ding Y, Wang Y, Liu X, Babu R, Ravis W, Yan W. Codelivery of Zoledronic Acid and Doublestranded RNA from Core-Shell Nanoparticles. Int J Nanomed. 2013; 8:137–145.

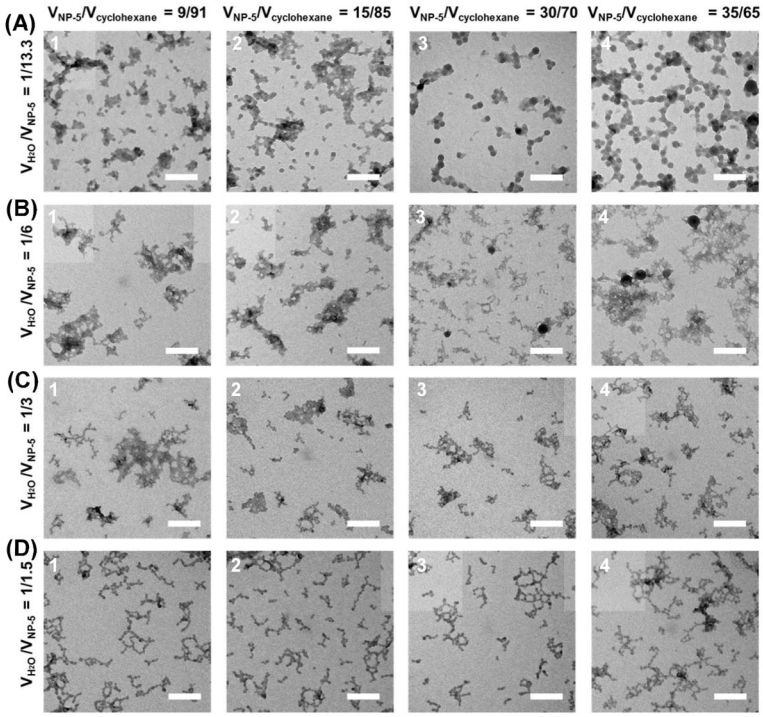

Figure 1.

Effect of the component ratios in reverse microemulsions (RM) consisted of H_2O, NP-5 (as the surfactant) and cyclohexane (as the oil phase) on Zol-Ca complexes synthesized. Shown are representative TEM micrographs of Zol-Ca complexes synthesized in RM system with fixed V_{H_2O}/V_{NP-5} ratios of 1/13.3 (**A**), 1/6 (**B**), 1/3 (**C**), or 1/1.5 (**D**) and different $V_{NP-5}/V_{cyclohexane}$ ratios, including 9/91, 15/85, 30/70 or 35/65 (bars = 100 nm).

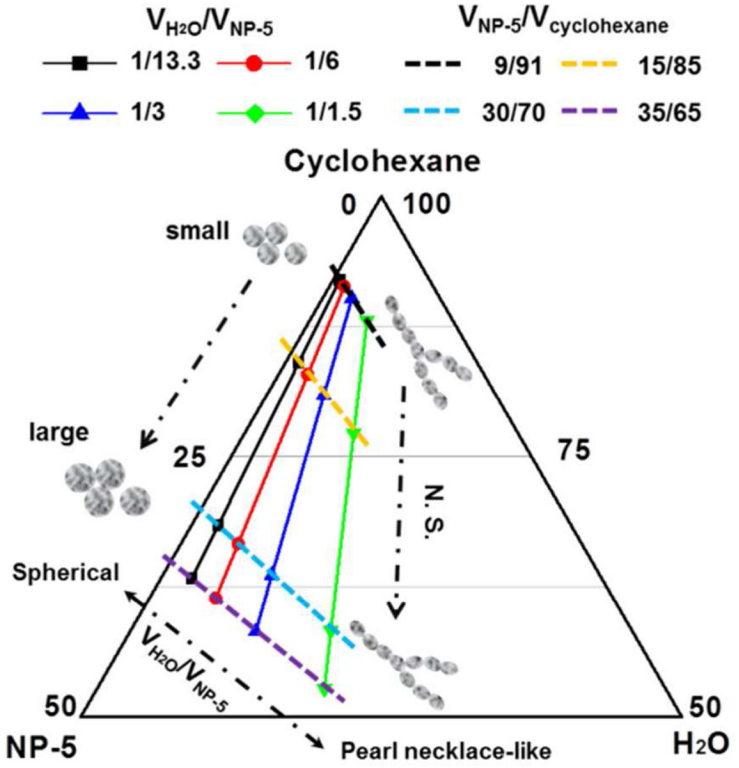

Figure 2.

Ternary phase diagram illustrating the relationship between the physical properties of Zol-Ca complexes synthesized and the volume ratios of H_2O, NP-5, and cyclohexane in the RM. Solid and dash lines represent the groups with fixed ratios of V_{H_2O}/V_{NP-5} and $V_{NP-5}/V_{cyclohexane}$, respectively (N.S. indicates no significant change).

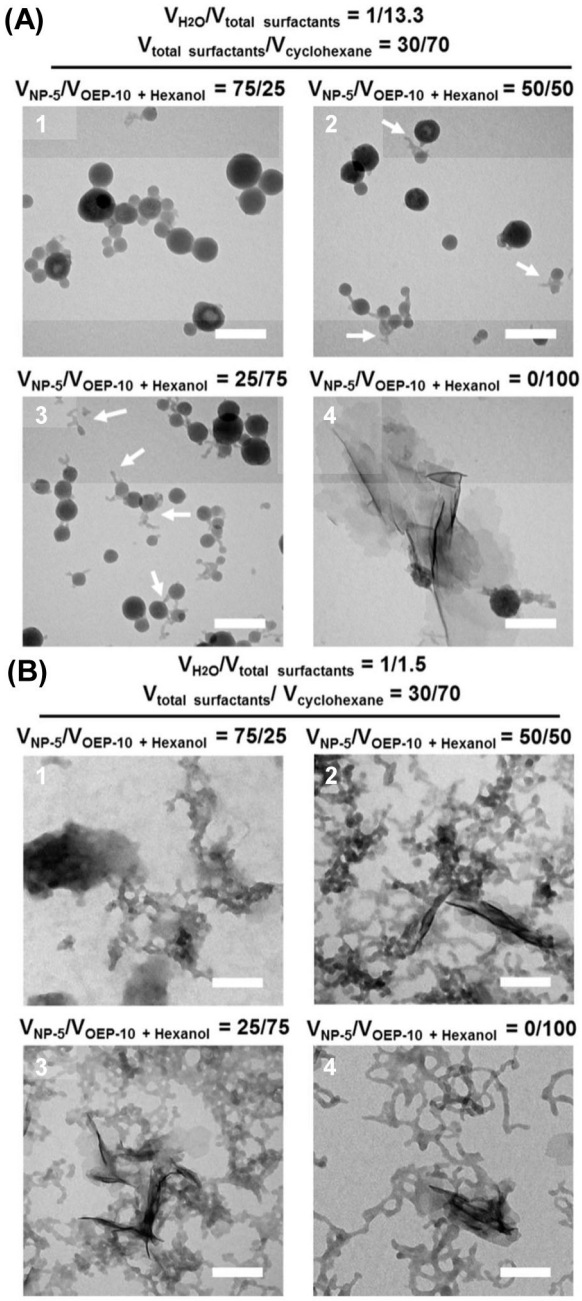

Figure 3.

Effect of the inclusion of co-surfactants in the RM on the physical properties of Zol-Ca complexes synthesized. Shown are representative TEM micrographs of Zol-Ca complexes synthesized using RM with both surfactant (NP-5) and co-surfactants (i.e. OEP-10 and Hexanol, 2:1, v/v). To describe the component ratio in the RM, the surfactant and co-surfactants are expressed together as total surfactants. The $V_{total\ surfactants}/V_{cyclohexane}$ ratio was fixed 30/70 and the $V_{H_2O}/V_{total\ surfactants}$ ratio was set as 1/13.1 **(A)** or 1/1.5 **(B)**. The $V_{NP-5}/V_{OEP-10\ +\ Hexanol}$ ratio was changed from 75/25 to 0/100. In **A-2** and **A-3**, products with irregular shape are indicated by white arrows (bars = 100 nm).

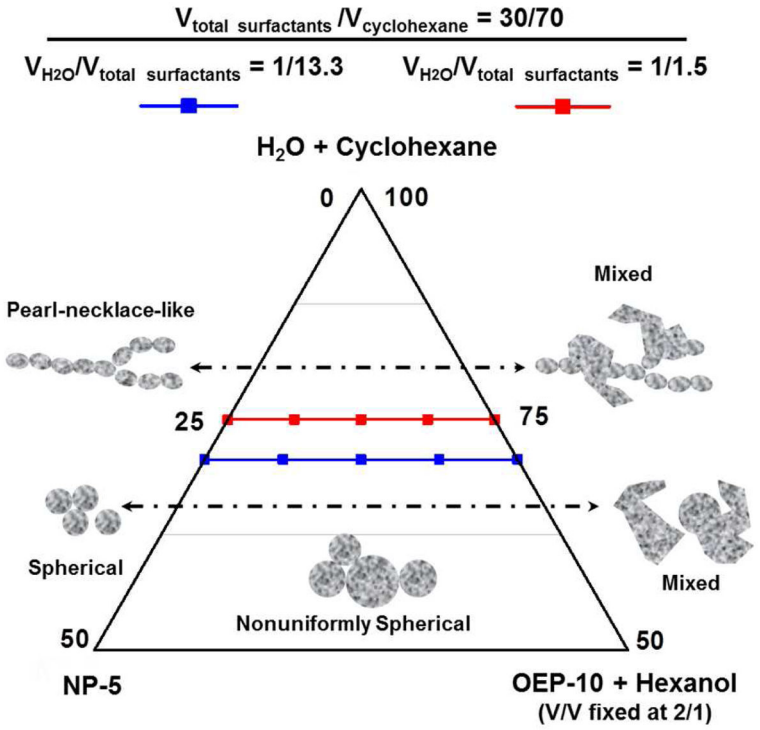

Figure 4.

Ternary phase diagram correlating the physical properties of Zol-Ca complexes synthesized and the volume ratio of surfactant (NP-5)/co-surfactants (OEP-10 and hexanol, 2:1, v/v) in RM. For simplicity, H_2O and cyclohexane are treated as one component. Red and blue lines indicate the groups with $V_{H_2O}/V_{\text{total surfactants}}$ ratios of 1/13.3 and 1/1.5, respectively.

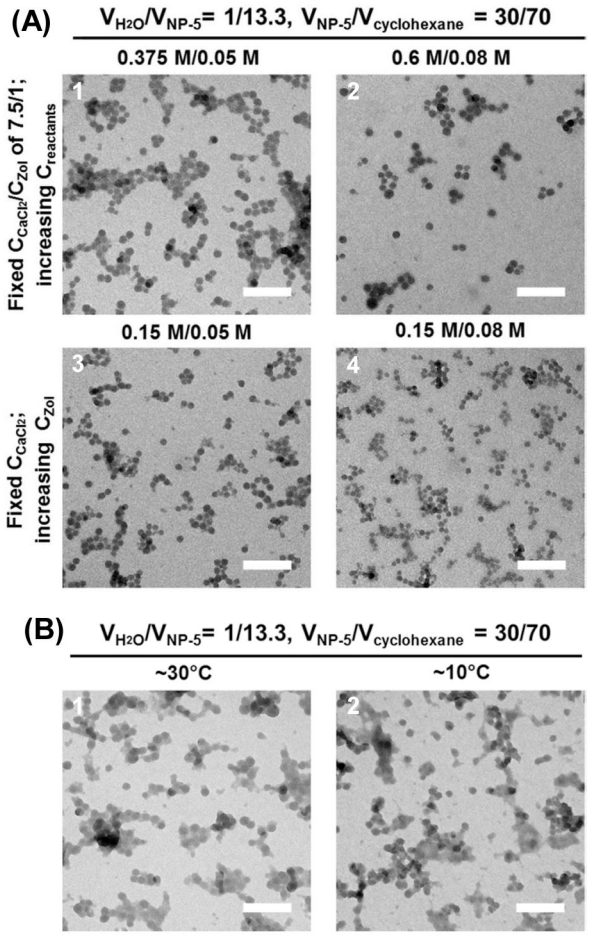

Figure 5.

Effects of reactant concentrations and reaction temperature on the physical properties of Zol-Ca complexes synthesized in RM. **(A)** Representative TEM micrographs of Zol-Ca complexes synthesized in RM with a fixed concentration ratio of $CaCl_2$/Zol at 7.5/1, but different concentrations of $CaCl_2$ and Zol (i.e. 0.375 M/0.05 M **(A-1)** or 0.6 M/0.08 M **(A-2)**); or with a fixed $CaCl_2$ concentration of 0.15 M, but different concentrations of Zol (i.e. 0.05M **(A-3)** or 0.08M **(A-4)**). **(B)** Representative TEM micrographs of Zol-Ca complexes synthesized in RM with a reaction temperature of ~30 °C or ~10 °C (bars = 100 nm).

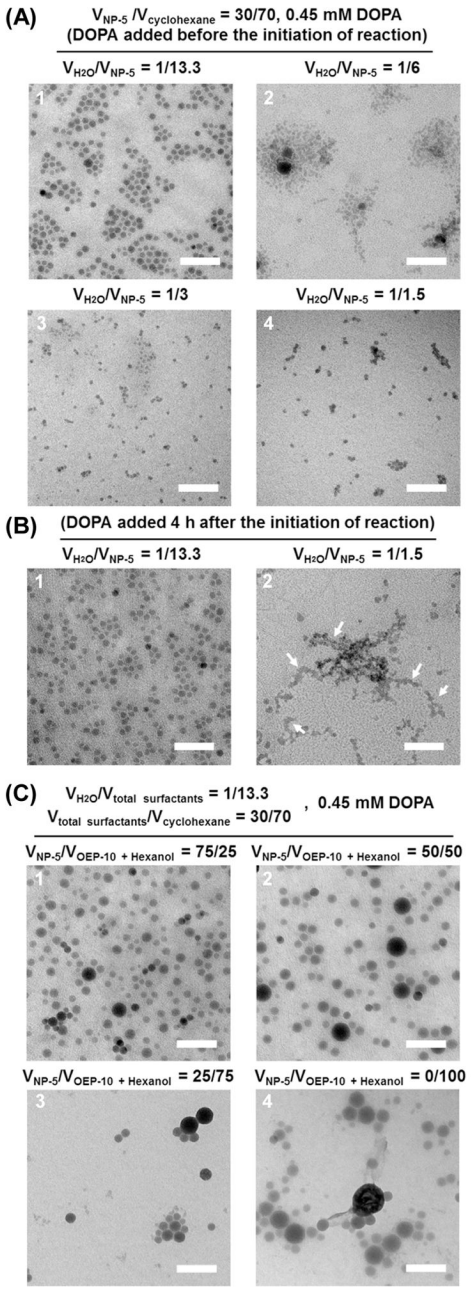

Figure 6.

Effect of phospholipid DOPA on the properties of Zol-Ca complexes synthesized in RM with different component ratios. **(A-B)** Representative TEM micrographs of Zol-Ca complexes synthesized in H_2O/NP-5/Cyclohexane RM_1 systems with 0.45 mM DOPA. **(A)** The RM has a fixed $V_{NP-5}/V_{cyclohexane}$ ratio of 30/70, but different V_{H_2O}/V_{NP-5} ratios, ranging from 1/13.3 to 1/1.5; DOPA was added into the RM before the initiation of reaction. **(B)** The RM has a fixed $V_{NP-5}/V_{cyclohexane}$ ratio of 30/70, but different V_{H_2O}/V_{NP-5} ratios of 1/13.3 **(B-1)** or 1/1.5 **(B-2)**; DOPA was added into RM 4 h after the initiation of reaction. **(C)** Representative TEM micrographs of Zol-Ca complexes synthesized in the RM_2 system

that contains co-surfactants (OEP-10 and hexanol, 2/1, v/v), with $V_{H_2O}/V_{\text{total surfactants}}$ and $V_{\text{total surfactants}}/V_{\text{cyclohexane}}$ ratios fixing at 1/13.1 and 30/70, respectively; the $V_{\text{NP-5}}/V_{\text{OEP-10 + Hexanol}}$ ratio was changed from 75/25 to 0/100 (bars = 100 nm).

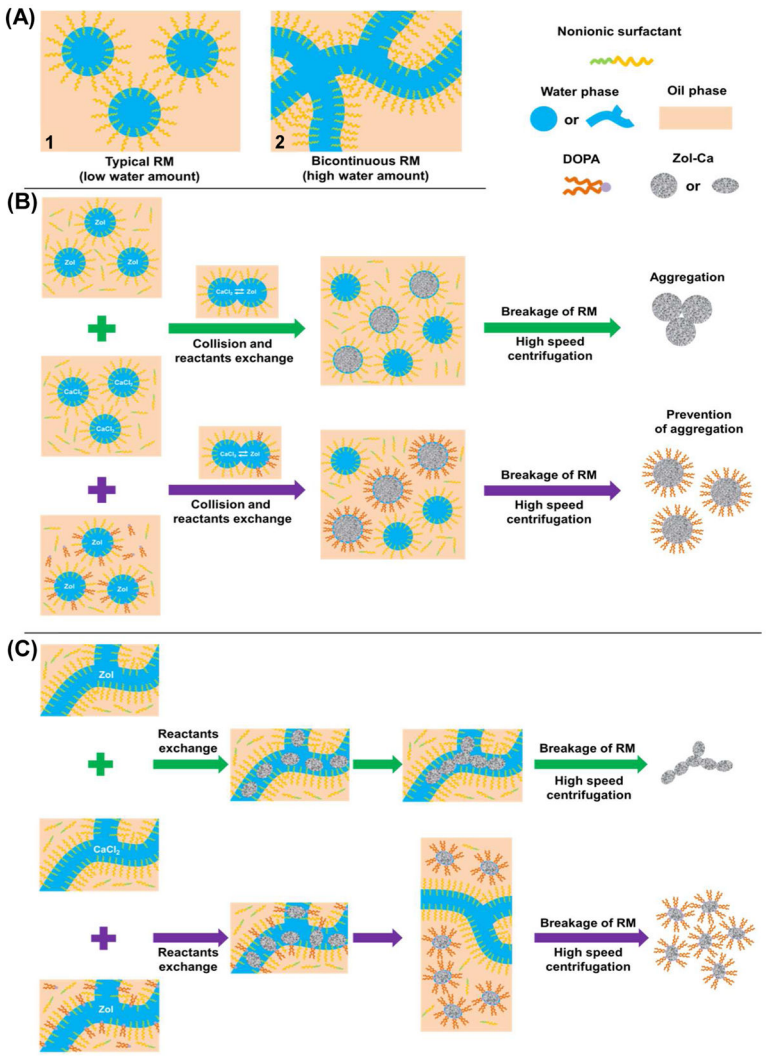

Figure 7.

Proposed mechanism of the formation of Zol-Ca complexes with different physical properties in RM. **(A)** Schematic diagrams of the typical RM with isolated sphere-like water phase (i.e. spherical droplets) **(A-1)**, or the bicontinuous RM with zig-zag channel-like water phase **(A-2). (B-C)** Proposed formation process of Zol-Ca complexes within typical RM with isolated sphere-like water phase **(B)** or within bicontinuous RM with zig-zag channel-like water phase **(C)** in the presence (purple arrow) or absence (green arrow) of DOPA.

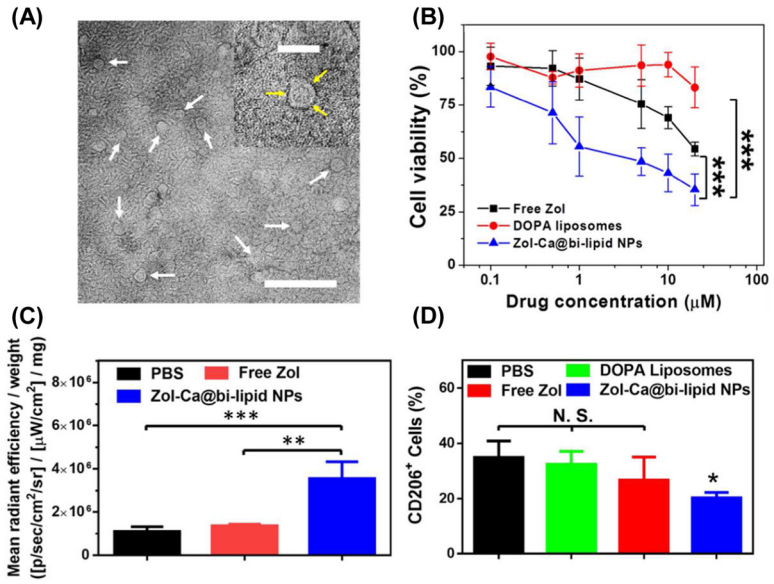

Figure 8.

Characterization and in vivo distribution of a new nanoparticle formulation of Zol (i.e. Zol-Ca@bi-lipid NPs). **(A)** A representative TEM micrograph of the Zol-Ca@bi-lipid NPs after negative staining. The bar represents 200 nm, and Zol-Ca@bi-lipid NPs with clear "core-shell" structure are indicated by white arrows. Shown in inset is the enlarged TEM image of one Zol-Ca@bi-lipid NP (bar = 50 nm) and the mixed lipid layer surrounded on the surface of Zol-Ca complex is indicated by yellow arrows. **(B)** In vitro cytotoxicity of Zol-Ca@bi-lipid NPs to J774A.1 murine macrophages after 48 h of incubation. Data are mean ± S.D. (n = 6, ***$p < 0.001$). **(C)** Mean fluorescent intensity of AF647-labeled Zol in M-Wnt tumors normalized by tumor weight. M-Wnt tumors were collected 24 h after mice were injected (i.v.) with Zol-Ca@bi-lipid NPs, free Zol, or PBS (2% of Zol was labeled with AF647). Data are mean ± S.D. (n = 4, ** $p < 0.01$, *** $p < 0.001$). **(D)** Effects of Zol-Ca@bi-lipid NPs on TAM population in orthotopic M-Wnt mammary tumors. Mice were i.v. injected with Zol-Ca@bi-lipid NPs 36 and 38 days after tumor cell inoculation. As controls, mice were injected with free Zol, PBS, or DOPA liposomes. Forty-eight hours after the second injection, mice were euthanized to collect tumors and the percent of $CD206^+$ cells in tumors was measured using flow cytometry. Data are mean ± S.D. (n = 3,* $p < 0.05$, as compared to the groups of PBS and DOPA liposomes).